Electronic Supporting Information

Methane synthesis from CO_2 and H_2O with concentrated NaOH–KOH electrolyte at 200–250 °C using electrochemical Pd–Ag membrane reactor.

Received 00th January 20xx,
Accepted 00th January 20xx

DOI: 10.1039/x0xx00000x

Wakana Seki,[a] Raisei Sagara,[a] Aika Hirata,[a] and Jun Kubota*[a]

Experimental details and numerical data that were not included in the main text are provided in the Electronic Supporting Information.

1. Analysis of produced gas using gas chromatograph

The gas composition at the reactor outlet was analyzed using a gas chromatograph (GC, GL Sciences GC-3210) equipped with a thermal conductivity detector (TCD). The chromatographic column was packed with Porapak Q (Waters Co.), and Ar was used as the carrier gas. The column pressure was maintained at 300 kPa during operation. The column oven temperature was set at 120°C. Gas samples were introduced using a gas sampling loop equipped with a 6-way valve. The TCD unit was kept at 180°C and 50 mA of current was applied.

The gases analyzed were CH_4, H_2, CO, and CO_2, whereas H_2O was not analyzed. A mixed gas containing equal amounts of CH_4, H_2, CO, and CO_2 was prepared, and the gas chromatogram of this mixture was measured to determine the relative sensitivities of the gas chromatograph for each gas, i.e., the response factors. The response factors for CH_4, H_2, CO, and CO_2 are shown in Table S1, which were normalized with respect to hydrogen (H_2 = 1). No corrections were applied for linearity with respect to concentration in the quantification; however, in this study, the overall current efficiency was approximately 100%, and the uncertainty in the CO_2 feed rate, which forms the basis of the production rate, was relatively large. Therefore, this omission is not considered to be problematic.

The concentration ratios of each gas component in the product gas were calculated by multiplying the peak areas of each component in the chromatogram by the corresponding response factors.

Some researchers appear to question the linearity between gas concentration and GC peak area intensity. Therefore, Fig. S1 shows the relationship between the mole fraction and the corresponding GC peak area signal obtained when sampling mixtures of CO_2 and H_2 using the GC system employed in this study. As the fraction and signal intensity exhibit an almost proportional relationship, quantitative analysis was performed on this basis.

There is no reasonable basis to doubt that linearity between concentration and peak area intensity is maintained for other combinations of gas species examined in this study. In gas chromatography, at sufficiently high concentrations, molecules with relatively high boiling points and strong polarity may undergo intermolecular association or oligomerization, potentially altering detector response and thereby compromising linearity.

2. Blank test without Ru/C catalyst

Fig. S2 shows gas chromatogram traces of the product gas from the membrane electrochemical cell operated at 250°C and 10 mA cm^{-2} with a CO_2 flow rate of 0.018 mL_{STP} min^{-1} cm^{-2}, without (A) and with (B) 300 mg of 30 wt%-Ru/C catalyst. All currents, formation and flow rates are normalized to the cathode geometric area. based on cathode geometric area.

In the absence of the catalyst (Fig. S2A), two distinct GC peaks were clearly observed: the peak appearing at ca. 1.8 min was assigned to H_2, and the peak at ca. 2.8 min to CO_2. As expected, when no catalyst was present, the H_2 produced by electrolysis was simply exhausted, and the fed CO_2 passed through the cell without conversion. In contrast, four peaks corresponding to H_2, CO, CH_4, and

Table. S1 Response factors of gases in GC.

H_2	CO	CH_4	CO_2
1.000	0.118	0.324	0.0930

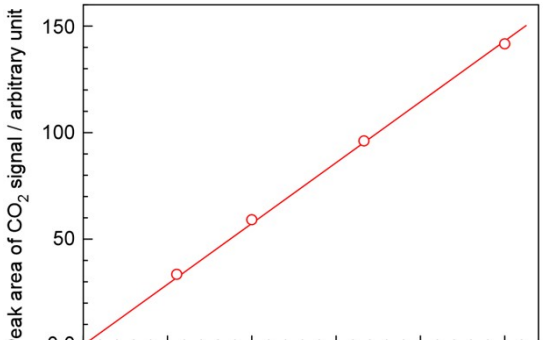

[a] *Department of Chemical Engineering, Fukuoka University, 8-19-1, Nanakuma, Jonan-ku, Fukuoka 814-0180, Japan.*
E-mail: jkubota@fukuoka-u.ac.jp (Jun Kubota)

CO_2 were observed in the exhaust gas from the catalyst-loaded cell (Fig. S2B).

Fig. S2B is presented as an example in which CO was detected in the gas chromatogram; however, no CO was detected at 250 °C under the conditions shown in Figs. 3 and 4 in the main text. In the experiment corresponding to Fig. S2B, the CO_2 flow rate was slightly higher than the stoichiometric requirement, which resulted in the observation of CO. When the CO_2 flow rate is accurately controlled, CO is not detected at 250°C, except under low-temperature conditions, as shown in Figs. 3 and 4.

Furthermore, a gas chromatogram of the cathode exhaust obtained under the open-circuit condition, that is zero current density, in which only CO_2 was supplied to the cathode side at 0.018 mL_{STP} min^{-1} cm^{-2} without applying any current, is presented in Fig. S2C. As expected, only CO_2 was detected, and no H_2 or CH_4 was observed.

Some researchers have suggested that the formation of CH_4 may originate not from the supplied CO_2 and H_2O but from impurities or from the materials used in the cell. However, the production rate reported in this study corresponds to a current efficiency of 90% at a current density on the order of a few hundred mA cm^{-2}. There are numerous reports in the literature in which products derived from impurities or cell components were mistakenly identified as target products, leading to erroneous claims of successful synthesis. In contrast, the production rate and current efficiency achieved in the present work clearly demonstrate that our results are fundamentally different from such cases.

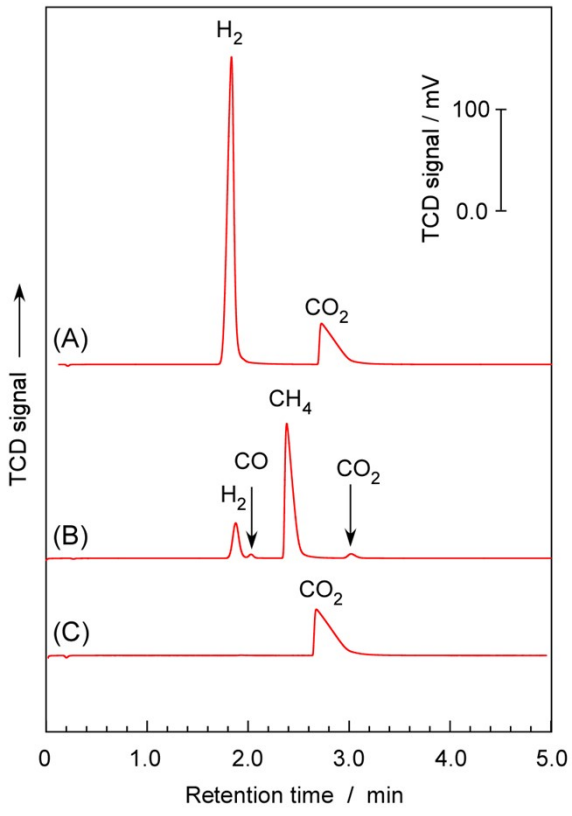

Fig. S2 Representative raw gas chromatograms obtained at 250°C under atmospheric pressure at a current density of 10 mA cm^{-2} with a CO_2 flow rate of 0.018 mL_{STP} min^{-1} cm^{-2}. The cell was equipped without (A) and with (B) 300 mg of 30 wt%-Ru/C catalyst. Trace (C) shows the GC profile measured for a cell loaded with a Ru/C catalyst at 250 C under a flow of 0.18 mL_{STP} min^{-1} cm^{-2} of CO_2, with no current applied. All currents, formation and flow rates are normalized to the cathode geometric area. based on cathode geometric area.

3. Gas cross-leak

In this study, a deviation of the overall current efficiency from 100% was attributed to cross-leakage of either O_2 or H_2. However, some researchers appear to assume that, if cross-leakage occurs, O_2 should be detected in the cathode exhaust gas or H_2 should be detected in the anode exhaust gas. As is evident from Fig. S2, O_2 has never been detected in the cathode exhaust under any operating conditions.

In the electrochemical membrane reactor employed in this study, the electrolysis cell compartment and the cathode gas compartment are completely isolated by a Pd-Ag metallic membrane. Even if O_2 were to diffuse toward the cathode side, it cannot permeate through the Pd-Ag metal membrane. Instead, O_2 would simply be reduced (hydrogenated) at the cathode interface and recombined to H_2O.

On the other hand, it may be considered possible that H_2 generated at the cathode diffuses toward the anode side and mixes into the anode exhaust gas. Fig. S3 shows the gas chromatogram of the anode exhaust obtained during methane synthesis at a current density of 50-300 mA cm^{-2}. At 300 mA cm^{-2}, cross-leakage is obvious. H_2O vapor

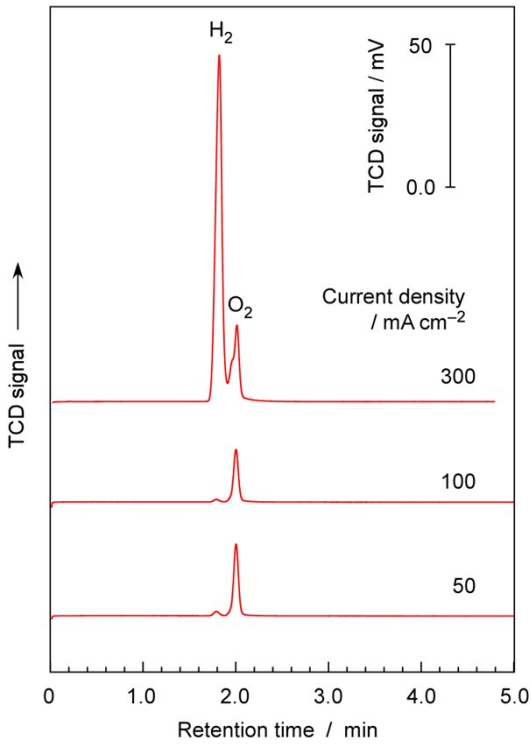

Fig. S3 Gas chromatogram for the anode exhaust gas. The cell was operated at 250°C under atmospheric pressure at a current density of 50-300 mA cm^{-2}. All currents, formation and flow rates are normalized to the cathode geometric area. based on cathode geometric area.

Table S3 Original numerical data for the current-density dependence of product formation rates and current efficiencies shown in Fig. 4 in the main text.

Current densites (mA cm^{-2})	Rate of formation (nmol s^{-1} cm^{-2})		CE (%)	
	H_2	CH_4	H_2	CH_4

was introduced to the anode side using Ar as the carrier gas, and Ar was also used as the GC carrier gas; therefore, Ar cannot be detected. In addition, H_2O condenses along the transfer line and, moreover, the GC column used in this study does not separate H_2O. Consequently, only the O_2 peak was observed in the chromatogram, and small amount of H_2 was detected.

It should be noted that the response factor of O_2 was only 0.118 when that of H_2 was defined as 1.000. Thus, although the GC peak of H_2 appears intense, the actual H_2/O_2 ratio was as shown in Fig. 7 in the main text.

Table S2 Original numerical data for the temperature dependence of product formation rates and current efficiencies shown in Fig. 3 in the main text.

Temp. (°C)	Rate of formation (nmol s^{-1} cm^{-2})			*CE* (%)		
	H_2	CO	CH_4	H_2	CO	CH_4
90.0	1.10	0.788	0.895	0.425	0.304	1.38
110	1.88	0.992	3.70	0.726	0.383	5.71
130	2.53	0.360	11.9	0.975	0.139	18.4
150	2.69	0.233	15.9	1.04	0.090	24.6
170	2.33	0.751	20.6	0.899	0.290	31.9
190	6.75	0.000	50.4	2.61	0.000	77.8
210	6.50	0.000	58.7	2.51	0.000	90.7
230	9.21	0.000	62.9	3.56	0.000	97.2
250	9.99	0.000	61.9	3.86	0.000	95.5

4. Calculation of formation rates

The production rates of each component were calculated as follows. As described in Section 1 above, the fractions of each component in the exhaust gas from the cell can be determined by GC analysis. The molar feed rate (mol s^{-1} cm^{-2}) of the introduced CO_2 can be calculated by dividing its volumetric flow rate by 22400 mL mol^{-1}. Because the total amount of CH_4, CO, and c discharged from the cell corresponds to the molar feed rate of the introduced CO_2, the discharge rates of CH_4, CO, and CO_2 can be calculated according to their respective fractions in the exhaust gas. The molar production rate of H2 can also be determined from its fraction relative to the production rates of the other components.

Because this calculation method is based on the assumption that carbon balance is maintained, it has the drawback that losses such as leakage of a portion of the introduced CO_2 or absorption into the electrolyte are not reflected in the results. However, if part of the CO_2 were lost or absorbed by the electrolyte, the H2 production rate would be underestimated, and the overall current efficiency would deviate from 100%.

5. Raw numerical data

The original numerical data for in Figs. 3 and 4 in the main text are listed in Table S2 and S3 respectively. The experimental conditions are described in Figs. 3 and 4 of the main text. If numerical data are required, please obtain them from this table. If a large amount of additional original data beyond those provided here is needed, please request them directly from the authors.

6. Photographs of apparatus

Because the schematic diagram in the main text may not clearly convey the experimental setup, photographs of the actual cell and apparatus are provided in Fig. S4.

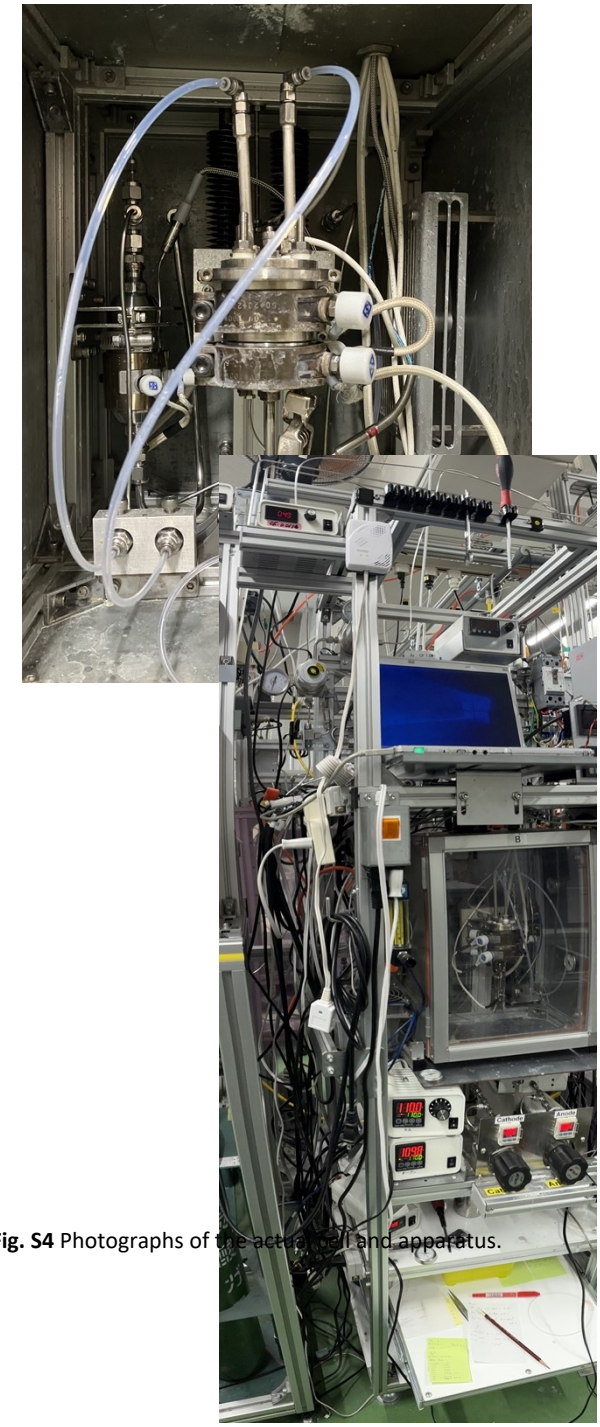

Fig. S4 Photographs of the actual cell and apparatus.